J Therm Anal Calorim (2012) 109:797–806
DOI 10.1007/s10973-012-2447-7

TG–DTG–DTA in studying white self-compacting cement mortars

V. Petkova · V. Stoyanov · Y. Pelovski

Bretsznajder Special Chapter

Abstract Self-compacting cement mortars and concretes are characterized with an excellent workability and with high early strengths, which makes them suitable for elements in pre-cast concrete. Both the dense structure and the non-defected surface of self-compacting mixes are achieved by the incorporation of relatively large amounts of fine mineral additives and use of polycarboxylate admixtures. All these advantages determine the great potential for manufacturing of architectural elements and details. However, there exist many features in the structure-formation and the hardening of these systems. The authors investigate in this study the evolution of the process of curing and the crystal formation up to the 120th days of water-curing. Moreover, the effects of replacement of 10 wt% white cement with natural zeolite are studied. Special attention is paid to the thermal analysis through which one determines the effects of dehydration of the new-formed crystal hydrates, de-carbonization of carbonate-containing phases, and zeolite incorporation. Differences in the thermal behaviour of self-compacting mortars are compared with two types of referent samples. The thermal experiments were complemented with physical–mechanical and structural measurements, including mercury intrusion porosimetry, powder X-ray diffraction and scanning electron microscopy. Experiments and analysis, both determining the development of the microstructure, indicate the formation of a dense structure of white self-compacting mortars. This is achieved at the early age impeding the growth of new crystals. The incorporation of zeolite increases the early strengths of samples, thus making the structure denser, and completely blocking the water permeability. As the zeolite is a soft and ductile mineral, it can be expected that the volume deformations of microstructure of the zeolite-containing mortars, are reduced.

Keywords Self-compacting mortar · Natural zeolite · White cement · Cement hydration · Thermal decomposition

Abbreviations

SCM	Self-compacting cement mortars
XRD	Powder X-ray diffraction
MIP	Mercury intrusion porosimetry
SEM	Scanning electron microscopy
W/P	Water-to-powder ratio
HRWR	High range water reducer
C–S–H	Calcium silicate hydrate

Introduction

Self-compacting are the non-segregating concretes that are compacted under the action of its own mass force. The macrostructure of the fresh concrete consists of two-phased coarse aggregates, which is dispersed in the cement mortar that determines the specific properties of this concrete [1].

V. Petkova (✉)
Institute of Mineralogy and Crystallography, Bulgarian Academy of Sciences, Acad. G. Bonchev Str., Block 107, 1113 Sofia, Bulgaria
e-mail: vilmapetkova@gmail.com

V. Stoyanov
Institute of Mechanics, Bulgarian Academy of Sciences, Acad. G. Bonchev Str., Block 4, 1113 Sofia, Bulgaria

V. Stoyanov
European Polytechnical University, 23 St. St. Kiril i Metodiy Str. 23, 2300 Pernik, Bulgaria

Y. Pelovski
University of Chemical Technology and Metallurgy, 8 Kl. Ohridski Str, 1756 Sofia, Bulgaria

The composition of the self-compacting cement mortar (SCM) is characterized with (i) a large diversity of water-reducing admixtures, (ii) a high content of powders (cement and fine mineral particles, sized below of 125 μm), (iii) a low water-to-powder (W/P) mass ratio, and (iv) a high paste volume. The hydration, setting and hardening of the SCM differ from those of the conventional cement-based mortars. Owing to its excellent workability, high early strengths, dense micro- and macrostructure and smooth non-defect surface [2–6], SCM offer many advantages for producing decorative and architecture pre-cast products with aesthetical surface.

Our previous studies [7] have showed that the SCM of white cement, white marble aggregate (of a 1:2 mass ratio) and polycarboxylate admixture have a strength value similar to that of the considered aggregate. Moreover, the fully non-defect surface had been formed where the fresh mix is in contact with a rigid surface (e.g. on the walls of the mould) [7, 8]. Substituting a relatively small amount of white cement with natural zeolite increases the density of the structure by acquiring an antique colour [8]. At a maximal dosage of the admixture of 2 % (as recommended by the manufacturer), a maximal amount of the substitution of white cement with zeolite of about 10 wt% was obtained, which value is limited to the appearance of surface defects [7].

The evaluation of physical–mechanical properties and durability of the white SCM studied is strongly hampered by both the complex mixture composition and the complicated processes of hydration in the system. Important for the structure-formation are (i) the mineral composition of the white cement, which differs from that of ordinary Portland-cements, (ii) the crystal texture of the marble particles, which differs from that of the quartz aggregates or milled limestone, (iii) the specific interaction of zeolite with water and reviling of pozzolanic properties, and (iv) the polycarboxylate admixture allowing a strong water reduction due to its electrostatic and steric effects.

DTA and TG are among the best methods for studying the structure of cement mortars and the roles of both the slow pozzolanic reactions and the influence of admixtures [9–12]. They are used for investigation of the hydration of white cements [13], of role of carbonate fillers [14–17], the advantages of addition of zeolite [18–21], and the structural changes of SCM at elevated temperatures [22–24].

In this article, by means of physical–mechanical measurements, thermal methods, XRD and SEM, we study the structure and the formation of the newly crystal phases in white SCM, and reveal the influence of marble aggregate, zeolite and polymer admixture on them.

Experimental

Raw materials

The white Portland cement employed was CEM I 52.5N (according to European Standards EN 197-1:2011 [25]), produced by Devnya Cement (Bulgaria). The mineral composition of the white cement was calculated using Bogue's method based on the chemical compositions given in Table 1 (in wt%): Ca_3SiO_5 (C_3S)—72.13; β-Ca_2SiO_4 (C_2S)—15.28; $Ca_3Al_2O_6$ (C_3A)—5.23; $Ca_4Al_2Fe_2O_{10}$ (C_4AF)—0.61. The other parameters used in this calculation were as follows: loss on ignition—2.8 %; insoluble residue in HCl and Na_2CO_3 (EN 196-2, §9:2006)—0.32 %; content of sulphuric anhydride—2.6 %; Blaine specific surface—4446 $cm^2\ g^{-1}$; compressive strength after 28 days—56.2 N/mm^2; water demand—30 %, soundness (Le Chatelier)—1.0 mm; and whiteness of 80.1 %.

As aggregate, we used a marble white-powder, which according to the producer, AIAS S.A. White Marble Products (Greece), has dolomitic consistence of about 95 wt%. In addition, our XRD analysis indicated that marble contains Mg-rich calcite. The maximal size of aggregate grains was 2 mm, 50.0 wt% of them being with sizes below 0.125 mm, and 5.0 wt% below 0.063 mm.

The clinoptilolite-based zeolite under study is obtained from Beli Plast deposit (Bulgaria) and has maximal particle size of 0.8 mm, specific density of 2.15 g/cm^3, bulk density of 0.81 g/cm^3, and absorbed water of 68 cm^3 per 100 g.

As a high range water reducer (HRWR), we used a polycarboxylate with density 1.07 g/cm^3 at 20 °C (provided by Sika ViscoCrete 5-800).

This super-plasticizer is soluble in water, chloride-free, light brown in colour, and without any retarding effects. The manufacturer's recommended dosage of HRWR for self-compacting concrete was 1.0–2.0 % of the mass of cement (or of cementations materials).

Table 1 Chemical composition of raw materials/wt%

Component	Main mineral	SiO_2	Al_2O_3	Fe_2O_3	CaO	MgO	Na_2O	K_2O	Other
White Portland cement	–	24.3	2.1	0.2	68.3	0.3	0.13	0.02	Free lime—1.9
Marble aggregate	Dolomite	0.12	0.38	0.14	32.9	20.0	0.05	0.19	$CO_2 + H_2O$—45.7
Natural zeolite	Clinoptilolite	66.15	11.31	0.67	4.20	0.46	0.34	3.13	H_2O—13.92

Mortars preparation and properties

Four mortars with the compositions given in Table 2 were studied. The mix design of SCMs (type A and B) was predetermined by the DOE method using D-optimal plan [7].

The mortars C and D were prepared via a procedure described in EN 196-1:2005.

The SCM was homogenized for a long time (up to for 120 s) with high speed to obtain self-levelling behaviour [27]. Two of the mortars had spread diameter, close to target values of 240–260 mm [26]. The content of distilled water of the reference mortars (type C and D) was chosen equal to the maximal possible value (0.6, corresponding to the greatest spreading diameter), at which a maximal spreading without any sedimentation and segregation has been achieved.

Three batches were prepared for each mortar and then cast into 40 × 40 × 160 mm moulds. These test specimens were moulded without any compaction (jolting or vibration). After 24 h of curing at RH > 95 % and 20 °C, they were de-moulded and immersed in water at 20 °C until the age of testing (from 1 to 120 days).

We measured the following physical–mechanical properties of the mortars: bulk density after immersion, spreading diameter, water adsorption after immersion, flexural and compressive strengths at 28 days and compressive strength at 120 days [28]. The method of measuring and the average values of these properties are shown in Table 3. Owing to the differing density of samples, the adsorption after immersion is calculated in volume percentages.

Experimental methods

The methods used to study both the curing and the effect of cement substitution with natural zeolite include thermal methods, mercury intrusion porosimetry (MIP), powder XRD [29–31], and SEM.

The structure of mortars was investigated on water-curing samples (for mortar type A, B at 1, 2, 3, 14, 28 and 120 days, and for mortar type C, D at 28 and 120 days), when the hydration had been stopped. For this purpose, monolithic pieces were cut from specimens of about 15 mm in size. Then, these samples were dried for 12 h at 50 °C and immersed in pure ethanol (99.9 %) for 3 days. Finally, the pieces were dried for again for 12 h in a forced-air oven at 50 °C.

For SEM studies, pieces with approximately flat surfaces of about 10 × 10 mm, while for MIP samples with a mass of 2.0 ± 0.3 mg were used. Powder XRD and thermal measurements were carried out on samples, prepared from about 50 g of dried material after grinding and completely sifting through a No. 200 mesh sieve (sieve size

Table 2 Codes and composition of mortars

Mortar type	Mass ratios					Ratios/(wt/wt)		
	Cement	Zeolite	Filler	Distilled water	HRWR	Water/cement	Water/binder*	Water/powder**
A						0.40	0.4	0.235
B	0.9	0.1	2.0	0.4	0.02	0.44	0.4	0.235
C	1.0	–	2.0	0.6	–	0.60	0.6	0.353
D	0.9	0.1	2.0	0.6	–	0.66	0.6	0.353

* Binder—white cement and zeolite

*** Powder—all particles with sizes below 125 μm

Table 3 Physical and mechanical properties of studied mortars

Property	Method	Units	Mortar type			
			A	B	C	D
Bulk density after immersion	[27]	kg/m^3	2348	2330	2158	2133
Spreading diameter	[25]	mm	332	290	135	118
Adsorption after immersion	[27]	mm^3/cm^3	192.5	162.4	258.5	277.0
28 days flexural strength	[26]	N/mm^2	11.51	9.79	8.11	7.43
28 days compressive strength	[26]	N/mm^2	90.1	98.3	53.8	51.4
120 days compressive strength	[26]	N/mm^2	106.2	109.0	61.5	61.7

0.075 mm) at minimum of 20 cycles. The average mass of the samples was 10.0 ± 0.2 mg for thermal analysis and 1.0 ± 0.1 mg for XRD.

Simultaneous TG–DTG–DTA analyses were carried out using a thermal analyser STA 780, Stanton Redcroft (England). The samples were heated from 20 to 1,000 °C at a constant rate of 10 °C min^{-1} in air flow of 50 cm^3 min^{-1}.

The XRD patterns were obtained on an X-ray powder diffractometer D2 Phaser Bruker AXS, with CuKα radiation ($\lambda = 0.15418$ nm) operating at 30 kV, 10 mA scanned from 5 to 70° 2θ with a step of 0.05°. The MIP was carried out using a Carlo Erba, Porosimeter Mod. 1520. In the pressure range 1–150 atm, corresponding to pore sizes ranging from 50 nm to 15000 nm. The SEM was performed on a Philips PH Model 515 in the regime of a secondary electron emission on flat surface coated with a thin layer of gold.

Thermal characterization of raw materials

White cement is characterized by loss of mass below 5 %, a part of which due to the dehydration of both crystal water (taking place below 220 °C) and structural water from the decomposition of $Ca(OH)_2$ and C–S–H phases, and the other to the de-carbonization of calcite. The mass losses of the thermal decomposition of the marble aggregate are due mainly to the de-carbonization of dolomite which proceeds in two sequential stages of decomposition at 800–860 °C having mass losses close to the theoretical. The total mass losses of zeolite are 12.3 % and are associated with the dehydration of the crystal and structural water of clinoptilolite [31]. As a result of the decomposition, the skeleton structure of zeolite gets broken leading to the formation of Al_2O_3, CaO, and MgO (Table 5).

Results and discussion

XRD

The phases identified in the hardened mortars are shown in Table 4.

All the SCMs, studied at different number of days of curing, contain the initial components of white cement (belite, plagioclase and calcite). This incomplete hydration is explained by the lack of water in SCM and/or the dissolution of clinoptilolite in mortars B and D. Portlandite is formed in the first days of curing and present in the samples during all periods of the process. The formation of thaumasite and ettringite is due to the presence of sulphate ions, while that of hemi- and mono-carboaluminate is due to the presence of carbonate ions. Thaumasite and hemicarboaluminate are formed during the first days of hydration, while ettringite and monocarboaluminate are identified in samples cured at least 7 days in water.

Table 4 The phases found out by XRD

No	Description	Phases
1	Non-hydrated phases of cement	Belite–Ca_2SiO_4
		Plagioclase—$(Na,Ca)Al(Si,Al)_3O_8$
2	Phases in the raw materials	Dolomite—$CaCO_3.MgCO_3$
		Mg-rich calcite—$CaCO_3$
		Quarz—SiO_2
3	New phases	
	CO_3^{2-}-containing	Mono- and hemi-carboaluminate – $3CaO{\cdot}Al_2O_3{\cdot}CaCO_3(OH)_{12}{\cdot}5H_2O$
		$3CaO{\cdot}Al_2O_3{\cdot}0.5Ca(OH)_2{\cdot}0.5CaCO_3{\cdot}5.5H_2O$
	SO_4^{2-}-containing	Thaumasite—$3Ca(OH)_2{\cdot}Si(SO_4)_2{\cdot}12H_2O$
		Ettringite—$6Ca(OH)_2{\cdot}Al_2(SO_4)_3{\cdot}26H_2O$
		$CaSO_4{\cdot}xH_2O$
	Hydrosilicates formed of CaO, Al_2O_3, SiO_2	Hillebrandite—$CaSiO_3{\cdot}Ca(OH)_2$
		Xonotlite—$5CaO{\cdot}6SiO_2{\cdot}Ca(OH)_2$
		Yugawaralite—$CaO{\cdot}Al_2O_3{\cdot}6SiO_2{\cdot}4H_2O$
	Si-free and Al-free hydrated phases	Portlandite—$Ca(OH)_2$

The usage of marble white aggregate (dolomite and Mg-rich calcite) increases the content of carbon ions [32]. These ions are a prerequisite to the formation of substituted in an isomorphic way carbonate-containing thaumasite [33, 34] and ettringite [35], following the hydration reactions in cement mortars:

$$6Ca^{2+} + 2AlO_2^- + 3CO_3^{2-} + 3SO_4^{2-} + 6OH^- + 26H_2O \rightarrow 3Ca(OH)_2{\cdot}3CaCO_3{\cdot}Al_2(SO_4)_3{\cdot}26H_2O \quad (1)$$

$$3Ca^{2+} + HSiO_3^- + CO_3^{2-} + SO_4^{2-} + OH^- + 14H_2O \rightarrow 3Ca(OH)_2{\cdot}Si(SO_4{\cdot}CO_3){\cdot}12H_2O \quad (2)$$

The C–S–H crystal-hydrates form thaumasite, ettringite, hillebrandite, xonotlite, yugawaralite, hydrogarnet as well as both mono-carboaluminate and hemi-carboaluminate. Our XRD data indicate that the phases containing hydroxyl ions are portlandite, hillebrandite and xonotlite (Table 4).

The replacement of 10 wt% cement with zeolite (mortars B and D) changes the cement hydration. Thus, hillebrandite and xonotlite have not been indicated in samples cured for 120 days in water, which may be explained by partial consumption of hydroxyl ions by zeolite [36] leading to a reduction of the amount of portlandite.

Both zeolite and marble particles affect the formation of a variety of calcium hydro-silicates in SCM. The

dissolution of clinker minerals in the presence of dolomite increases quickly the pH of the solution, the highly alkaline solution allowing the dissolution of zeolite tuff and the formation of anions, following the reactions [37]:

$$\equiv \text{Si-O-Si} \equiv + 6\text{OH}^- \rightarrow 2\left[\text{SiO(OH)}_3\right]^- \quad (3)$$

$$\equiv \text{Si-O-Al} \equiv + 7\text{OH}^- \rightarrow \left[\text{SiO(OH)}_3\right]^- + \left[\text{Al(OH)}_4\right]^- \quad (4)$$

The formation of centres of crystallization is possible from broken octahedral as well as tetrahedral fragments from the skeleton structure of zeolite and from the Ca^{2+} from cement. This allows growing of hydrated calcium aluminosilicate compounds, illustrated partially by the reactions [36, 37]:

$$6\text{Ca}^{2+} + 2\left[\text{Al(OH)}_4\right]^- + 4\text{OH}^- + 3\text{SO}_4^{2-} + 26\text{H}_2\text{O} \rightarrow 6\text{Ca(OH)}_2\cdot\text{Al}_2(\text{SO}_4)_3\cdot 26\text{H}_2\text{O} \quad (5)$$

$$3\text{Ca}^{2+} + \left[\text{SiO(OH)}_3\right]^- + 2\text{SO}_4^{2-} + \text{OH}^- + 10\text{H}_2\text{O} \rightarrow 3\text{Ca(OH)}_2\cdot\text{Si(SO}_4)_2\cdot 9\text{H}_2\text{O} \quad (6)$$

SEM and MIP

The SEM images in Fig. 1 show the structure of the samples studied. It is obvious that the structure of SCM is denser than that of the conventional concretes [38, 39]. The replacement of 10 wt% of white cement with zeolite leads to the formation of shrinkage cracks caused by self-desiccation at these low water-cement ratios in the bulk of material (Fig. 1d, f).

The compressive strength of SCM is significantly greater than that of the mortars with a greater water-cement ratio (Table 3). The addition of zeolite increases the 28 day compressive strength of SCMs, this effect being opposite in the reference mortars. Despite the dense structure of mortars when immersed in water, the curing of SCM continues. The measured increased compressive strength and the evolution of the total porosity of SCM (Fig. 2) are comparable to that of mortars C and D.

The pores in the SCM are interconnected with voids and cracks through which the water can penetrate deeply in the material, thereby continuing the processes of hydration and crystallization. The cohesion fracture in sample B (Fig. 1b)

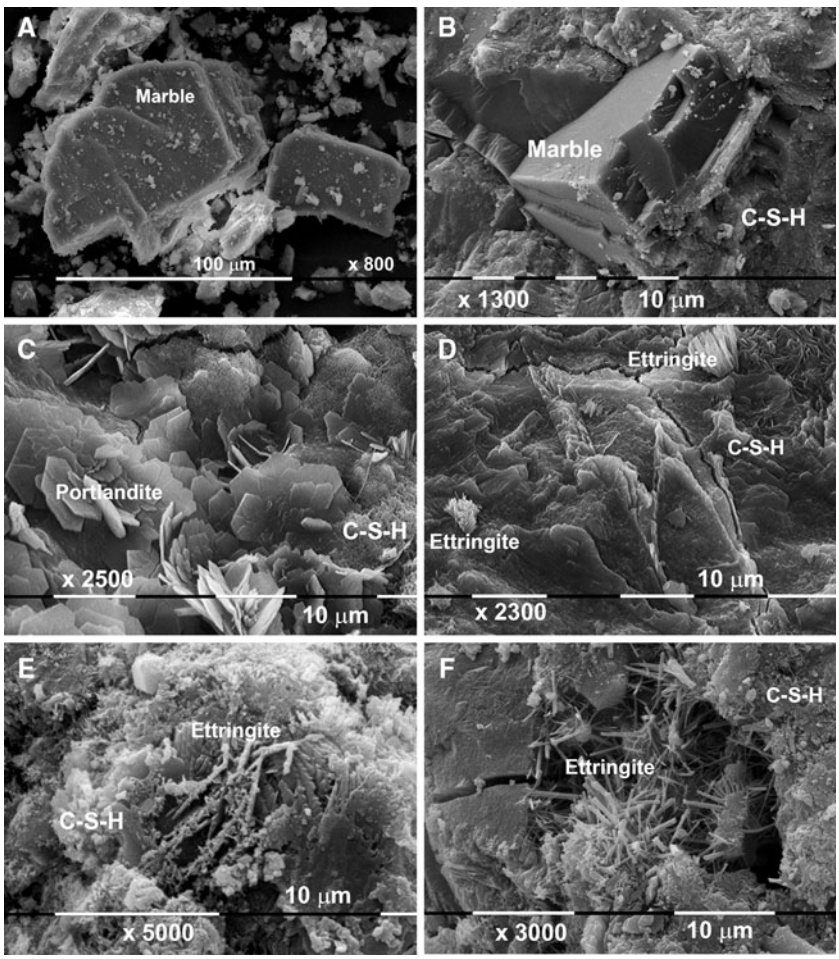

Fig. 1 SEM micrographs of: **a** raw particles of marble aggregates; **b** a broken particle of marble aggregates of mortar B at 120 days curing; **c** surface of mortar A at 120 days curing; **d** surface of mortar B at 120 days curing; **e** surface of mortar C at 28 days curing; **f** surface of mortar D at 28 days curing

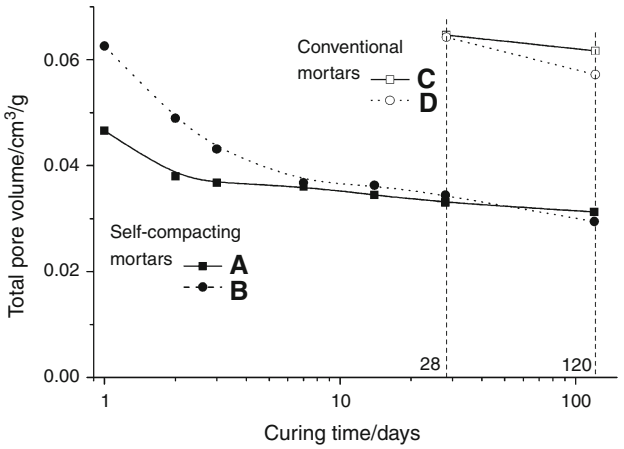

Fig. 2 Evolution of the total volume of pores during curing of mortars in water

proves that the compression strength of the SCM is close to the possible maximum, limited by the strength of the marble aggregate. An additional explanation of the increase in compressive strength is the pozzolanic activity of zeolite, the active amorphous phases, SiO_2 and Al_2O_3, of which react with the portlandite forming variable additional C–S–H crystals.

The morphology of the samples indicates that dissolution and hydration of cement minerals have proceeded only partially. When the cement minerals dissolute in the absence of zeolite (Fig. 1c, e), the surface is covered with a variety of plate crystals of portlandite, needle-like crystalline ettringite and small crystals of C–S–H gel and other crystalline products grown in the voids between portlandite particles. The replacement of 10 wt% of cement with zeolite (Fig. 1d, f) impedes the cement hydration due to lack of water. The products of hydration in the absence of both portlandite and ettringite cover only a small part of the surface and shrinkage cracks appear.

The C–S–H gel is with finer crystalline structure and with interpenetrating crystal forms, a picture corresponding to our XRD data (Table 4).

TG–DTG–DTA

Results of the thermal studies of the investigated samples are shown in Figs. 3, 4, and 5, whereas the characteristic values for the raw solid materials and used mortars are given in Table 5. The data concerning the mass losses are presented into three temperature regions: (I) from 40 to 200 °C; (II) from 430 to 470 °C and (III) from 540 to 830 °C, which are analysed separately.

Region I (40–200 °C)

In this region, the crystal water dehydration of the new-formed calcium silicate hydrates, is dominated. The small mass losses indicate a low content of crystal water. The thermal behaviour of the samples may be divided into four

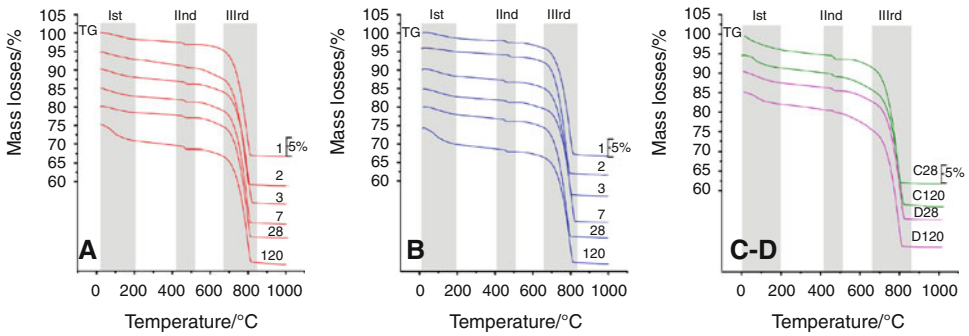

Fig. 3 TG curves of mortars *A*, *B*, *C* and *D*

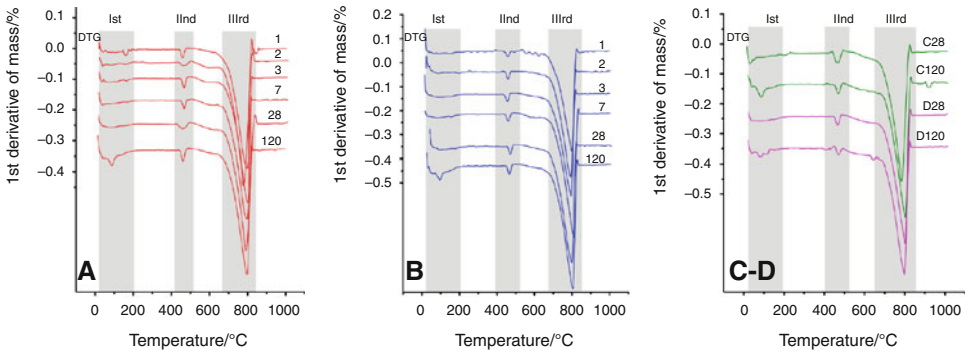

Fig. 4 DTG curves of mortars *A*, *B*, *C* and *D*

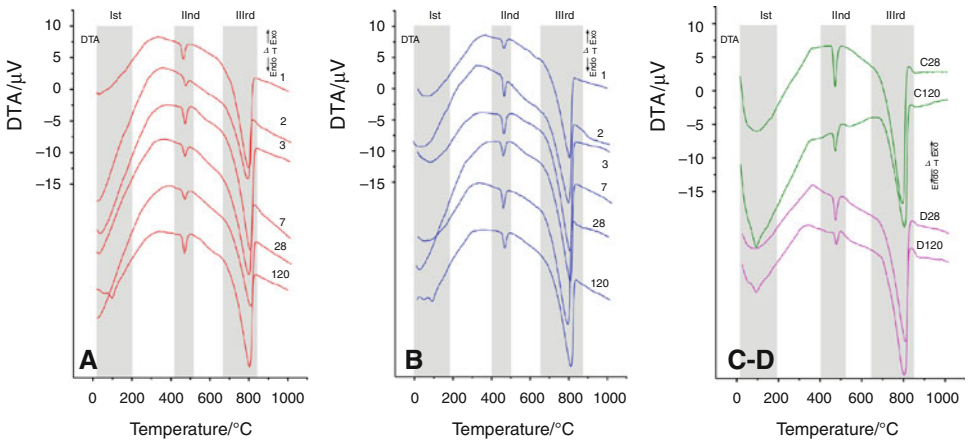

Fig. 5 DTA curves of mortars *A*, *B*, *C* and *D*

Table 5 Dynamics of the changes of mass losses and temperature ranges of the thermal decomposition of mortars

No	Sample/days of water-curing	Dehydration						$Ca(OH)_2$		C–S–H		Decarbonization		Total
		1		2		3								
		T_{inf}/°C	ΔG/%	T_{inf}/°C	ΔG/%	T_{inf}/°C	ΔG/%	T_{inf}/°C	ΔG/%	T_{inf}/°C	ΔG/%	T_{inf}/°C	ΔG/%	ΔG/%
Raw materials														
1.	Cement	65.8	0.28	99.0	0.39	279.4	0.27	430.5	0.24	539.6	0.60	710.3	3.28	5.17
2.	Marble	–	–	–	–	–	–	–	–	–	–	806.6	30.02	45.11
		–	–	–	–	–	–	–	–	–	–	821.2	15.14	
3.	Clinoptilolite	70.8	6.23	187.0	2.00	323.2	2.15	–	–	–	–	–	–	12.32
Mortar A, water-curing														
4.	1 day	40.9	0.18	84.8	0.99	161.1	0.50	459.5	0.57	609.3	0.84	795.8	29.02	33.30
5.	2 days	42.0	0.53	99.3	0.84	165.9	0.58	468.0	0.79	591.7	2.79	777.8	28.26	35.58
6.	3 days	40.3	0.46	82.4	1.14	167.6	0.47	469.4	0.69	574.6	2.52	804.1	29.68	35.83
7.	7 days	41.6	1.58	–	–	169.7	0.59	470.8	0.69	589.8	2.40	786.4	29.45	35.94
8.	28 days	45.0	1.06	90.7	1.04	160.3	0.65	457.9	0.64	609.9	2.22	790.0	29.43	35.19
9.	120 days	41.0	1.14	88.1	1.82	139.8	1.15	464.2	0.82	593.7	1.41	798.6	29.12	37.71
Mortar B														
10.	1 day	60.1	0.39	95.3	0.49	144.9	0.61	458.5	1.32	627.4	1.37	796.8	28.87	33.49
11.	2 days	–	–	90.4	0.42	137.8	0.34	460.5	0.61	526.2	1.43	787.7	30.00	33.10
12.	3 days	–	–	87.0	1.21	158.4	0.72	458.5	0.65	624.4	1.57	792.8	28.96	34.41
13.	7 days	40.2	0.54	88.8	0.96	160.0	0.66	464.2	0.55	583.8	1.81	803.9	30.03	35.67
14.	28 days	50.4	0.37	89.7	1.03	158.2	0.82	456.4	0.67	619.0	1.44	782.6	29.72	35.53
15.	120 days	44.7	0.98	90.3	2.13	141.8	1.07	464.3	0.66	589.3	0.77	802.1	29.05	36.76
Mortar C														
16.	28 days	35.0	1.29	85.0	1.71	198.6	0.69	466.1	1.07	602.7	2.18	782.5	28.88	37.67
17.	120 days	40.5	0.35	86.7	1.52	143.7	0.98	469.2	0.97	591.5	4.07	788.3	27.64	37.63
Mortar D														
18.	28 days	39.2	0.40	87.6	1.69	166.3	0.59	466.3	0.75	578.4	2.89	790.2	28.86	36.73
19.	120 days	41.1	0.59	83.1	1.10	115.8	0.78	468.0	0.73	541.5	1.38	791.0	28.78	39.13
										650.0	3.45			

sub-regions of endothermic effects (Fig. 6; Table 5). These results, obtained by physical methods and related to references, allow assuming four differing types of thermal effects (losses) connected with dehydration of:

- zeolite–water, 40–65 °C [19];
- ettringite, 75–90 °C [40];
- gypsum and thaumasite, 100–130 °C [40, 41];
- calcium silicate hydrate, 150–170 °C [42];

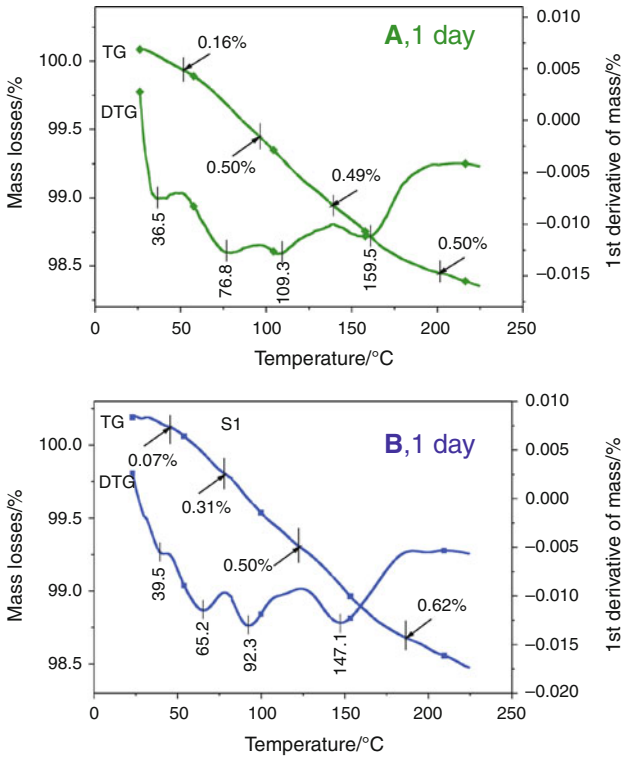

Fig. 6 TG–DTG of one-day-water-cured self-compacting mortars of type A (**a**) and of type B (**b**)

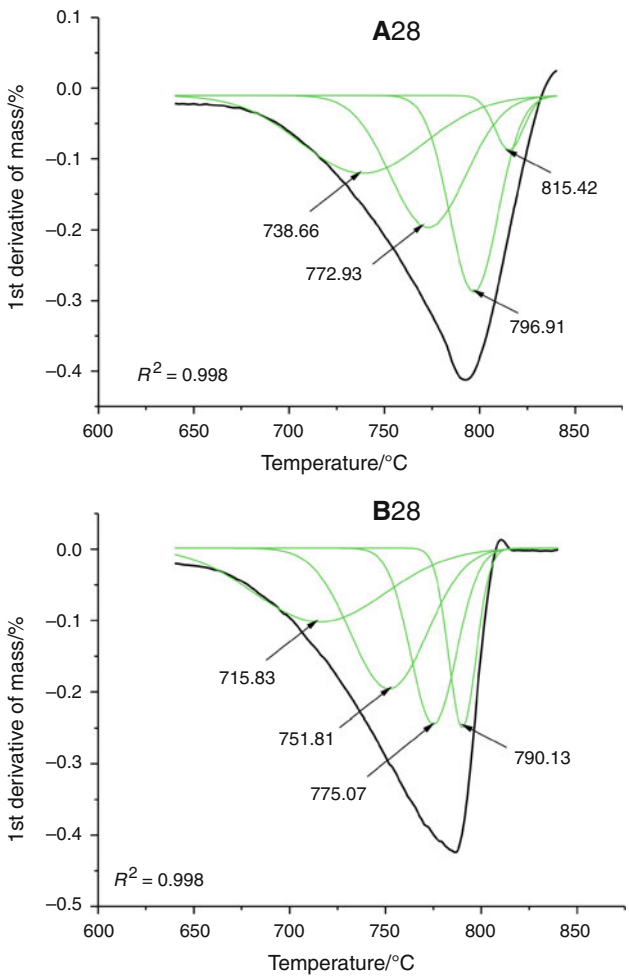

Fig. 7 Gaussian decomposition of the decarbonization peak for carbonate phases in the temperature range 660–740 °C: **a** mortar A at 28 days of curing, **b** mortar B at 28 days of curing

Region II (430–470 °C)

The reaction products of the hydration of the main cement minerals (alite and belite) are portlandite and C–S–H. In early period of hydration, the formation of portlandite dominates, but is undesirable phase in the concretes due to both its solubility in water and the formation of porous interfacial transition zone at the aggregate surface. Zeolite is a pozzolanic material because its amorphous constituents (SiO_2 and Al_2O_3) react with portlandite, forming insoluble C–S–H or C–A–S–H phases. This pozzolanic activity of zeolite can be estimated according to the simultaneous reduction of portlandite and the increase in the amount of calcium phases of C–S–H gel. The amount of portlandite was measured via the mass loses in the temperature region 430–470 °C (Figs. 3, 4, 5; Table 5).

Both the endothermic effects and the mass loss in this temperature range are associated with dehydration of the formed portlandite. This thermal process is a single stage at temperatures not related to other thermal reactions, and, thus, it can be used to evaluate the pozzolanic activity of zeolite [10, 42–45]. The data in Table 5 show that the temperature of dehydration of mortar B is slightly lower than those of the other samples. There is a tendency of reducing the mass losses on increasing the age (from 1 to 120 days), this being more noticeable for mortar B.

Region III (540–830 °C)

In this temperature range, both the thermal effects and the mass losses are associated with the crystal water decomposition of C–S–H (540–680 °C) and the decarbonization of dolomite, calcite and calcium carboaluminates (660–740 °C) (Figs. 3, 4, 5; Table 5) [44, 46, 47]. Due to the dense structure of SCM (Fig. 1) the quantity of crystal water is low, i.e. the mass losses are small and the registered endothermic effects are of a low intensity (Table 5). Nevertheless, a peak of maximum mass losses may be registered, which for mortar A is at the second day of curing, while for mortar with zeolite (mortar B) is at the seventh day. Thus, the amount of crystal water decreases, reaching its minimum at the end of the period studied. For the mortars A, B and D, the dependences shown in Figs. 5 and 6 are similar, while the registered losses for the reference mortar C, they are increased. In SCMs, the delayed

Table 6 Parameters of the Gaussian decomposition

Mortar	Days of curing	Peaks position/°C			
		I-st peak	II-nd peak	III-rd peak	IV-th peak
A	28	738.66	772.93	796.91	815.42
	120	706.27	762.05	787.76	806.48
B	28	715.83	751.81	775.07	790.13
	120	710.54	759.76	787.40	804.18
C	28	686.68	737.29	768.68	790.72
	120	683.37	757.30	786.35	803.35
D	28	686.02	756.05	785.87	803.95
	120	661.54	753.64	783.60	801.90

formation of C–S–H is difficult due to their dense structures (Fig. 1) and low porosity (Fig. 2).

The obtained DTG–DTA curves indicate that the decomposition of carbonate phases takes place in temperature ranges close to each other (Figs. 4, 5). As seen in Fig. 7, the DTG peaks in the temperature range of 660–740 °C vary in shape only and, to determine the number of the resulting phases and their temperature behaviour, we used decomposition through four Gaussian functions corresponding to carboaluminates (I), dolomite (II and III), and calcite (IV) (numbered according increase of temperatures).

The results obtained are presented in Table 6, and they show that the decarbonization temperatures for mortars A, B and C increase, whereas it is the lowest for mortar D. The reason is that the formed structure of the hardened mortars is very dense in the former case and is porous in the latter, leading to an increase in the temperature of decarbonization.

Conclusions

We suggest an optimal dose of a chemical additive which makes it possible to disperse easier both cement and aggregates particles. Thus, a faster and better wetting is proposed leading to a low water-to-powder ratio. It is found that both the added marble aggregate and zeolite contributes to the self-desiccation and the related autogenous shrinkage.

Regardless of the very dense structure, the SCMs have open and continuous porosity. Water penetrates through capillaries, thus allowing for realization of the processes of delayed hydration and pozzolanic reaction and reducing the amount of portlandite.

The hydration of white SCM is characterized with a low content of crystal water. The replacement of a part of the white cement with natural zeolite reduces the density of the hardened mortars, increasing at the same time, both the amount and the variety of the new crystalline phases.

The thermal decomposition proceeds into three temperature regions, 40–200 °C, 430–470 °C, and 540–830 °C. The DTA–TG–DTG studies confirm the low content of water in the mortars, which takes place in the first two temperature regions. The dense structure of SCM is revealed by an increase in the temperatures in the third region of decarbonization. The determined peaks allow one to evaluate the variety of carbonate-containing products in the mortars under study.

References

1. Forde MC, editors. ICE manual of construction. Thomas Telford Publishing; 2009. p. 928.
2. Corradi M. Concrete for the construction industry of tomorrow. In: Konsta-Gdoutos MS, editor. Measuring, monitoring and modeling concrete properties. Amsterdam: Springer; 2006. p. 429–40.
3. Sukumar B, Nagamani K, Srinivasa Raghavan. Evaluation of strength at early ages of self-compacting concrete with high volume fly ash. Constr Build Mater. 2008;22:1394–401.
4. Uysal M, Yilmaz K. Effect of mineral admixtures on properties of self-compacting concrete. Cement Concr Compos. 2011;33:771–6.
5. Parra C, Valcuende M, Gómez F. Splitting tensile strength and modulus of elasticity of self-compacting concrete. Constr Build Mater. 2011;25:201–7.
6. López A, Tobes JM, Giaccio G, Zerbino R. Advantages of mortar-based design for coloured self-compacting concrete. Cement Concr Compos. 2009;31:754–61.
7. Stoyanov V. Investigation of properties of decorative mortars besed on design of experiments In: Proceedings of the international conference on civil engineering design and construction. (Eurocodes – Science and Practice) DCB; 2010. p. 09–11.
8. Stoyanov V, Kolentzov S. Effects of fiber content on the properties of high-fluidity mortars for decorative applications. In: Barovsky N, editors. Proceedings of the 12th international conference on mechanics and technology of composite materials, Varna; 2009. p. 130–136.
9. Ramachandran VS. Elucidation of the role of chemical admixtures in hydrating cements by DTA technique. Thermochim Acta. 1972;4:343–66.
10. Roszczynialski W. Determination of pozzolanic activity of materials by thermal analysis. J Therm Anal Calorim. 2002;70:387–92.
11. Pacewska B, Blonkowski G, Wilińska I. Studies on the pozzolanic and hydraulic properties of fly ashes in model systems. J Therm Anal Calorim. 2008;94:469–76.
12. Ashraf M, Naeem Khan A, Qasair Ali, Mirza J, Goyal A, Anwar AM. Physico-chemical, morphological and thermal analysis for the combined pozzolanic activities of minerals additives. Constr Build Mater. 2009;23:2207–13.
13. Martínez-Ramírez S, Frías M. The effect of curing temperature on white cement hydration. Constr Build Mater. 2009;23(3):1344–8.
14. Tsivilis S, Kakali G, Chaniotakis E, Souvaridou A. A study on the hydration of Portland limestone cement by means of TG. J Therm Anal Calorim. 1998;52:863–70.
15. Péra J, Husson S, Guilhot B. Influence of finely ground limestone on cement hydration. Cement Concr Compos. 1999;21:99–105.
16. Darweesh HHM. Limestone as an accelerator and filler in limestone-substituted alumina cement. Ceram Int. 2004;30(3):145–50.

17. Zhang Y, Zhang X. Research on effect of limestone and gypsum on C_3A, C_3S and PC clinker system. Constr Build Mater. 2008;22(8):1634–42.
18. Janotka I, Krajči L'. Sulphate resistance and passivation ability of the mortar made from pozzolan cement with zeolite. J Therm Anal Calorim. 2008;94:7–14.
19. Kontori E, Perraki T, Tsivilis S, Kakali G. Zeolite blended cements: evaluation of their hydration rate by means of thermal analysis. J Therm Anal Calorim. 2009;96:993–8.
20. Perraki T, Kontori E, Tsivilis S, Kakali G. The effect of zeolite on the properties and hydration of blended cements. Cement Concr Compos. 2010;32:128–33.
21. Snellings R, Mertens G, Elsen J. Calorimetric evolution of the early pozzolanic reaction of natural zeolites. J Therm Anal Calorim. 2010;101:97–105.
22. Ye G, Liu X, De Schutter G, Taerwe L, Vandevelde P. Phase distribution and microstructural changes of self-compacting cement paste at elevated temperature. Cem Concr Res. 2007;37:978–87.
23. Bakhtiyari S, Allahverdi A, Rais-Ghasemi M, Zarrabi BA, Parhizkar T. Self-compacting concrete containing different powders at elevated temperatures—mechanical properties and changes in the phase composition of the paste. Thermochim Acta. 2011;514:74–81.
24. Fares H, Remond S, Noumowe A, Cousture A. High temperature behaviour of self-consolidating concrete: microstructure and physicochemical properties. Cem Concr Res. 2010;40:488–96.
25. EN 197-1:2011. Cement: part 1: composition, specifications and conformity criteria for common cements.
26. EFNARC. Specification and guidelines for self-compacting concrete. European federation for specialist construction chemicals and concrete systems, Norfolk (English ed.). The European Guidelines for Self Compacting Concrete; 2005.
27. EN 196-1:2005. Methods of testing cement—part 1: determination of strength.
28. ASTM C642. 06 standard test method for density, absorption, and voids in hardened concrete.
29. Richardson IG. The calcium silicate hydrates. Cem Concr Res. 2008;38:137–58.
30. Taylor R, Richardson IG, Brydson RMD. Composition and microstructure of 20-year-old ordinary Portland cement–ground granulated blast-furnace slag blends containing 0 to 100 % slag. Cem Concr Res. 2010;40:971–83.
31. Petkova V, Serafimova E, Petrova N, Pelovski Y. Thermochemistry of triboactivated natural and NH_4-exchanged clinoptilolite mixed with Tunisian apatite. J Therm Anal Calorim. 2011;105:535–44.
32. Matschei T, Lothenbach B, Glasser FP. The role of calcium carbonate in cement hydration. Cem Concr Res. 2007;37:551–8.
33. Taylor HFW. Cement chemistry. 2d ed. London: Thomas Telford Publishing; 1997.
34. Aguilera J, Martınez-Ramırez S, Pajares-Colomo I, Blanco-Varela MT. Formation of thaumasite in carbonated mortars. Cement Concr Compos. 2003;25:991–6.
35. Barnett SJ, Adam CD, Jackson ARW. Solid solutions between ettringite, $Ca_6Al_2(SO_4)_3(OH)_{12}{\cdot}26H_2O$, and thaumasite, $Ca_3Si(SO_4)CO_3(OH)_6{\cdot}12H_2O$. J Mater Sci. 2000;35:4109–14.
36. Perraki Th, Kakali G, Kontori E. Characterization and pozzolanic activity of thermally treated zeolite. J Therm Anal Calorim. 2005;82:109–13.
37. Perraki Th, Kakali G, Kontoleon F. The effect of natural zeolites on the early hydration of Portland cement. Microporous Mesoporous Mater. 2003;61:205–12.
38. Famy C, Brough AR, Taylor HFW. The C–S–H gel of Portland cement mortars: Part I. The interpretation of energy-dispersive X-ray microanalyses from scanning electron microscopy, with some observations on C–S–H, AFm and Aft phase compositions. Cem Concr Res. 2003;33:1389–98.
39. Balonis M, Glasser FP. The density of cement phases. Cem Concr Res. 2009;39:733–9.
40. Gruskovnjak A, Lothenbach B, Winnefeld F, Figi R, Ko S-C, Adler M, Mäder U. Hydration mechanisms of super sulphated slag cement. Cem Concr Res. 2008;38:983–92.
41. Drábik M, Tunega D, Balkovic S, Fajnor VŠ. Computer simulations of hydrogen bonds for better understanding of the data of thermal analysis of thaumasite. J Therm Anal Calorim. 2006;85(2):469–75.
42. Chaipanich A, Nochaiya Th. Thermal analysis and microstructure of Portland cement-fly ash-silica fume pastes. J Therm Anal Calorim. 2010;99:487–93.
43. Adams J, Dollimore D, Griffiths DL. Thermal analytical investigation of unaltered $Ca(OH)_2$ in dated mortars and plasters. Thermochim Acta. 1998;324:67–76.
44. Dollimore D, Gupta JD, Lerdkanchanaporn S Sr, Nippani A. Thermal analysis study of recycled portland cement concrete (RPCC) aggregates. Thermochim Acta. 2000;357–358:31–40.
45. Pacewska B, Wiliñska Iw, Bukowska M. Calorimetric investigations of the influence of waste aluminosilicate on the hydration of different cements. J Therm Anal Calorim. 2009;97(1):61–6.
46. Vessalas K, Thomas PS, Ray AS, Guerbois J-P, Joyce P, Haggman J. Pozzolanic reactivity of the supplementary cementitious material pitchstone fines by thermogravimetric analysis. J Therm Anal Calorim. 2009;97(1):71–6.
47. Jo Dwecka, Mauricio Buchler P, Coelho ACV, Cartledge FK. Hydration of a Portland cement blended with calcium carbonate. Thermochim Acta. 2000;346:105–13.